5642 *Biochemistry* **2010,** *49,* 5642–5650
DOI: 10.1021/bi1003553

BIOCHEMISTRY
including biophysical chemistry & molecular biology
Article

Molecular Insight into Intrinsic Heme Distortion in Ligand Binding in Hemoprotein[†]

Saburo Neya,*[,‡] Masaaki Suzuki,[‡] Tyuji Hoshino,[‡] Hirotaka Ode,[§] Kiyohiro Imai,[∥] Teruyuki Komatsu,[⊥] Akira Ikezaki,[#] Mikio Nakamura,[#] Yuji Furutani,[▽] and Hideki Kandori[●]

[‡]*Department of Physical Chemistry, Graduate School of Pharmaceutical Sciences, Chiba University, Inage-Yayoi, Chiba 263-8522, Japan,* [§]*Laboratory of Viral Genomics, Pathogen Genomics Center, National Institute of Infectious Diseases, Gakuen, Musashimurayama-shi, Tokyo 208-0011, Japan,* [∥]*Department of Material Chemistry, Faculty of Engineering, Hosei University, Koganei, Tokyo 184-8787, Japan,* [⊥]*Research Institute for Science and Engineering, Waseda University, Okubo, Shinjuku, Tokyo 169-8555, Japan,* [#]*Department of Chemistry, School of Medicine, Toho University, Ota-ku, Tokyo 143-8450, Japan,* [▽]*Institute of Molecular Science, Myodaiji, Okazaki 444-8585, Japan, and* [●]*Department of Material Science and Engineering, Nagoya Institute of Technology, Showa-ku, Nagoya 466-8555, Japan*

Received March 9, 2010; Revised Manuscript Received June 8, 2010

ABSTRACT: A pair of myoglobins containing inherently distorted α-ethyl-2,4-dimethyldeuteroheme or undistorted 2,4-dimethyldeuteroheme were prepared, and the functional consequence of intrinsic heme deformation was investigated. The visible absorption peaks of the myoglobin bearing the distorted heme exhibited a bathochromic shift, indicating that the heme was deformed in the protein pocket. Ligand affinities for the ferric myoglobin with the distorted heme were found to be higher than those of the myoglobin bearing the undistorted heme. The observation suggested that the iron atom was more displaced toward the proximal histidine to weaken the coordination of the water molecule. In the paramagnetic proton NMR spectrum of ferrous deoxy protein, the deformed heme caused a 3.2 ppm lower-field shift of the proximal histidine signal, supporting an enhanced iron−histidine interaction. The deformed heme in ferrous myoglobin lowered the oxygen and carbon monoxide affinities by 25- and 480-fold, respectively, and caused the cleavage of the iron−histidine bond in a fractional population of the nitric oxide derivative. These results demonstrate a distinctive controlling mechanism for ligand binding by the deformed heme. Upon the heme distortion, the iron atom is more attracted by the proximal histidine to reduce the affinity of exogenous ligands for the ferrous heme.

Heme is the prosthetic group in hemoprotein and essential for diverse functions such as oxygen transport, oxygen activation, electron transfer, and signal transduction. The characteristic coordination environments of hemoproteins direct the heme to the specific function. In peroxidase, for instance, the axial coordination of the partially deprotonated imidazole facilitates the generation of the high-valent oxidation state, while reversible oxygenation in hemoglobin and Mb[1] is facilitated by the neutral proximal histidine.

Recently, the nonplanar heme deformation has been suggested to be important for the regulation of the physical properties of hemoprotein (*1*, *2*). When heme is placed in a crowded protein cavity, the heme is apt to be deformed from planar to nonplanar conformations (*3*). Heme deformation is also observed in synthetic hemes bearing numerous and/or bulky peripheral substituents (*1*−*4*). Deformed heme affects the coordination core constituted with four pyrrole rings to perturb the reactivity of chelating metal. An unusual intermediate-spin ($S = {}^3/_2$) state, for instance, is encountered in nonplanar ferric model hemes (*4*, *5*), horseradish peroxidase, and cytochrome *c*′ (*6*, *7*). Although the intermediate-spin state has been proposed to coincide with the high-spin ($S = {}^5/_2$) state by quantum-mechanical admixing (*6*), the recent IR analyses for the five-coordinate azide hemes indicate that the $S = {}^3/_2$ and ${}^5/_2$ states are actually in thermal equilibrium with a very rapid conversion rate of $10^{11}-10^{12}$ s^{-1} (*8*, *9*). The heme distortion also causes the red shift of the visible absorption bands, the decrease in the redox potentials, and the upfield shift of the *meso*-carbon NMR signals of porphyrin (*1*−*4*). Since notable heme deformation is found only in a limited number of hemoproteins that catalyze specific functions (*6*, *7*, *10*), a generalized view of the inherent heme deformation of the ligand binding in protein still remains to be developed.

The experimental evaluation of heme deformation in protein has been the subject of continuing interest, but the protein is not readily accessible; a valuable hemoprotein with deformed heme is prepared via genetic engineering (*10*). A simple protein system that widely opens the opportunity to analyze heme deformation would be desirable. For this purpose, a pair of prosthetic groups, α-ethyl-2,4-dimethyldeuteroheme (**1**) and 2,4-dimethyldeuteroheme (**2**) in Figure 1, were prepared and coupled with apoMb. Heme **1** was designed to induce built-in heme distortion by an ethyl substituent, and heme **2** was employed as an undistorted reference. The *meso*-ethyl group in heme **1** is expected to alter the geometry of heme and the reactivity of the reconstituted protein. The advantages of hemes **1** and **2** are threefold. First, both hemes bearing propionate groups are close analogues of natural heme and facilitate protein reconstitution. Second, because of the molecular symmetry about the α,γ *meso*-carbon axis, they are free from the orientation disorder which is frequently found in

[†]This work was supported in part by a grant-in-aid [(A)-20249072] from the Promotion of Science for Scientific Research, Japan, and by a grant-in-aid for Innovation Area (#2107) from MEXT, Japan, for T.K.

*To whom correspondence should be addressed. Phone: +81-43-290-2925. Fax: +81-43-290-2925. E-mail: sneya@p.chiba-u.ac.jp.

[1]Abbreviations: Mb, myoglobin; Tris, tris(hydroxymethyl)aminomethane; EPR, electron paramagnetic resonance; DSS, sodium 2,2-dimethyl-2-silapentane-5-sulfonate.

 Published on Web 06/10/2010

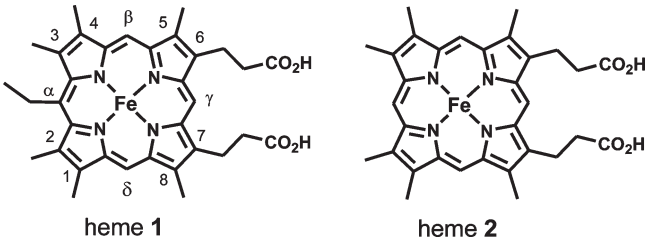

FIGURE 1: Structure of the hemes incorporated in a globin matrix.

asymmetric natural hemes (*11*). Third, the hemes without vinyl side chains avoid the complicating influences of the electron withdrawal and π-conjugation by vinyl groups. We demonstrate herein that the intrinsic heme distortion controls the ligand affinity of Mb in a peculiar manner.

MATERIALS AND METHODS

Hemes. 2,4-Dimethyldeuteroporphyrin dimethyl ester, a free macrocycle of heme **2**, was synthesized using the reported method (*12*) and identified via its proton NMR spectrum (*12*) and mass analysis.

We obtained α-ethyl-2,4-dimethyldeuteroporphyrin dimethylester (23 mg, 12% yield), a free macrocycle of heme **1**, with the method of Maruyama et al. (*13*) by coupling 100 mg of 1,1-bis(5-carboxy-3,4-dimethyl-2-yl)propane (*13*) with 250 mg of 5,5′-diformyl-3,3′-bis(2-methoxycarbonylethyl)-4,4′-dimethyl-2,2′-dipyrrylmethane (*14*). $C_{35}H_{42}N_4O_4$ requires: C, 72.20; H, 7.12; N, 9.42. Found: C, 71.97; H, 7.26; N, 9.33. Mass: *m*/*e* 594, calcd for M^+ for 594.7. ^{1}H NMR (chloroform-*d*): δ −3.02 (H, br s, NH), −2.90 (H, br s, NH), 1.83 (3H, t, -CH_2CH_3), 3.27 (4H, t, 2 × -$CH_2CH_2CO_2$-), 3.62, 3.63, and 3.64 (each 6H, s, 2 × ring -CH_3), 3.67 (6H, s, 2 × -CO_2CH_3), 4.36 (4H, t, 2 × -$CH_2CH_2CO_2$-), 5.21 (2H, q, -CH_2CH_3), 9.83 (H, s, *meso*-H), 10.09 (2H, s, *meso*-H). λ_{max} (and ε_{mM}) (chloroform): 406 (172), 505 (14.1), 538 (5.2), 573 (5.6), 625 (1.5) nm. The pK_3 of the pyrrole NH group of the porphyrin was determined by spectrophotometric titration in 2.5% sodium dodecyl sulfate (*15*). Iron was inserted into the heme dimethylesters (*16*). Alkaline hydrolysis of the ester groups (*17*) afforded the free acids of hemes **1** and **2**, which were precipitated with hydrochloric acid and dried under vacuum.

Reconstituted Protein. Sperm whale Mb was commercially available from Sigma (type II). The apoprotein prepared using the method of Asakura (*18*) was mixed with a 1.2-fold molar excess of the hydrolyzed ferric heme **1** or **2** in a minimum volume of 0.01 M NaOH (*18*). The crude mixture was dialyzed overnight against cold 10 mM Tris at pH 6.5 and loaded on a carboxymethylated cellulose column (Whatman, CM52) equilibrated with the same buffer. Reconstituted Mb was eluted from the column with a linear gradient from 0.01 to 0.10 M Tris buffer (pH 7.0). The typical yield of the reconstitution was ≥70%. The extinction coefficient of aquomet Mb**2** (ε_{mM}), the Mb containing heme **2**, was quantitatively determined to be 148 at 393 nm on the basis of the pyridine hemochromogen spectra of heme **2** (*19*). Aquomet Mb**1**, the Mb bearing heme **1**, was assessed with an ε_{mM} of 138 at 403 nm by the pyridine hemochromogen spectrum of heme **1**. λ_{max} (ε_{mM}): 396 (132), 521 (17.3), 551 (16.7) nm in a 1:3 (v/v) pyridine/0.1 M NaOH mixture in the presence of sodium dithionite.

Physical Measurements. Visible absorption spectra were recorded on a Shimadzu MPS-2000 instrument. IR spectra were recorded at 2 cm^{-1} resolution by using a 50 μm cell on a Digilab FTS-7000K instrument equipped with an Oxford cooling unit and apodized with a Happ-Genzel function. X-Band EPR spectra were recorded on a Bruker EMX spectrometer attached with an Oxford cryostat system. Proton NMR spectra at 400 MHz were recorded with a JEOL α400 spectrometer.

Quantum Chemical Calculation. Molecular structures of the ferric chloride derivatives of hemes **1** and **2** were optimized by quantum chemical calculation with Gaussian 03 (*20*). The B3LYP/6-311++G* level was applied to the calculation, and the potential energy of the optimized structure was estimated at the same level of theory.

Ligand Binding. The ligand binding constant was evaluated with spectrophotometric titration. A 3.5 mL portion of the Mb solution in a quartz cuvette was placed in the spectrophotometer equipped with a sample holder kept at 20 °C with a temperature-controlled water bath. The absorbance changes were recorded after addition of small portions (1−10 μL) of a ligand stock solution to the Mb. The equilibrium constant was determined with the plots of $1/\Delta A$ versus 1/[ligand]. The oxygen equilibrium curve was recorded on an automatic recording apparatus of Imai (*21*) in the presence of an enzymic reducing system (*22*). Flash photolysis of MbCO were performed on a Unisok TPS-1000WK time-resolved spectrometer with a Spectron Laser System SL803G-10 Q-switched Nd:YAG laser, which generated a second harmonic 6 ns pulse.

RESULTS

Porphyrin and Heme. Prior to a detailed account of the Mb containing synthetic heme, we characterized the prosthetic group itself. The optical titration of α-ethyl-2,4-dimethyldeuteroporphyrin with dilute hydrochloric acid in 2.5% sodium dodecyl sulfate at 20 °C showed Soret absorption changes with a decrease in pH. From the analysis of the spectral transition, we determined a pK_3 of 6.0 for the third protonation of the pyrrole nitrogen in this porphyrin. The value is comparable with the pK_3 of 5.9 reported for 2,4-dimethyldeuteroporphyrin (*23*). Visible absorption bands of the ferric chloride complexes of heme **1** (383, 510, 540, and 640 nm in chloroform) exhibited a slight bathochromic shift as compared with those (380, 506, 535, and 638 nm in chloroform) of heme **2**.

We optimized the molecular structure of ferric chloride hemes **1** and **2** with the quantum chemical calculations. The orientation of the ethyl group in heme **1** was assumed to be identical to that of the iron-bound chloride. Figure 2 illustrates the equatorial coordination environment and the deviation of the constituting atoms from the mean N_4 plane. Both hemes have similar in-plane structures except that the N_4 core of heme **1** possesses a slightly rectangular distortion. The average Fe−N(pyrrole) distance of 2.096 Å and the Fe−Cl length of 2.242 Å in heme **2** are close to the values of 2.062 and 2.218 Å, respectively, in protoporphyrin ferric chloride (*24*). The observation suggests the reliability of the calculation. In contrast, the heme planarity is distinctly different between the two. Heme **2** adopts a square-pyramidal or domed structure, all of the pyrrole carbons being on one side of the N_4 plane. This is typical of the five-coordinate ferric high-spin iron porphyrins, where the iron atom is displaced from the porphyrin plane toward the axial chloride atom (*25*). On the other hand, the introduction of a *meso*-ethyl group in heme **1** induced interesting structural variation. The influence was not localized but spread over the molecule. The four *meso*-carbons in heme **1** are alternatively above and below the N_4 plane, and the eight pyrrole α-carbons adopted twisted conformations against the heme plane. Heme **1** displayed both doming and ruffling distortions.

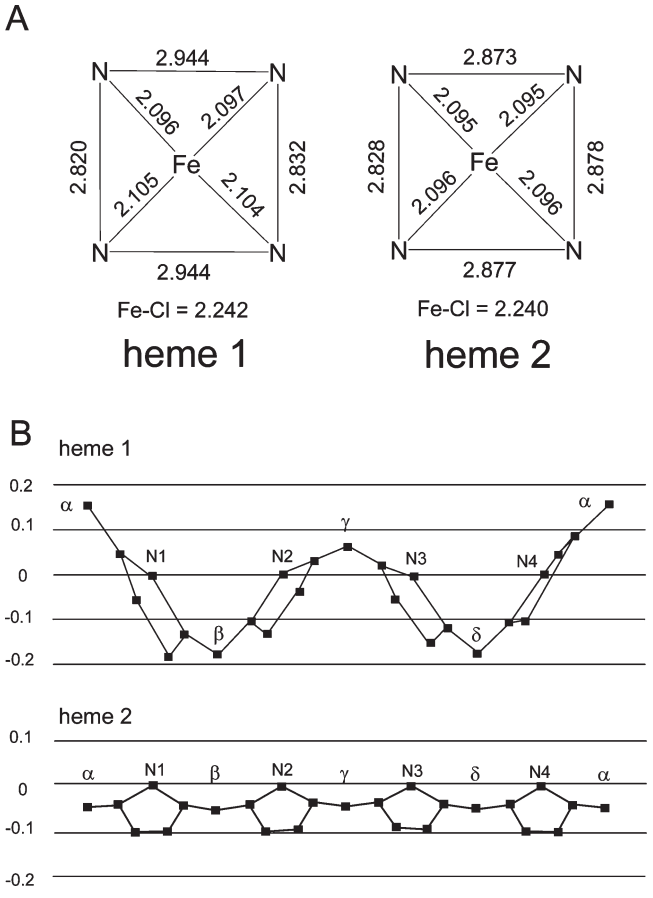

FIGURE 2: Minimum energy structures calculated for the ferric chloride complexes of hemes **1** and **2**. The calculation was performed by including all of the peripheral substituents. (A) Iron coordination structures. (B) Side view of the skeletal deviations from the N_4 plane for the porphyrin atoms in ferric hemes **1** and **2**. The values are in angstroms.

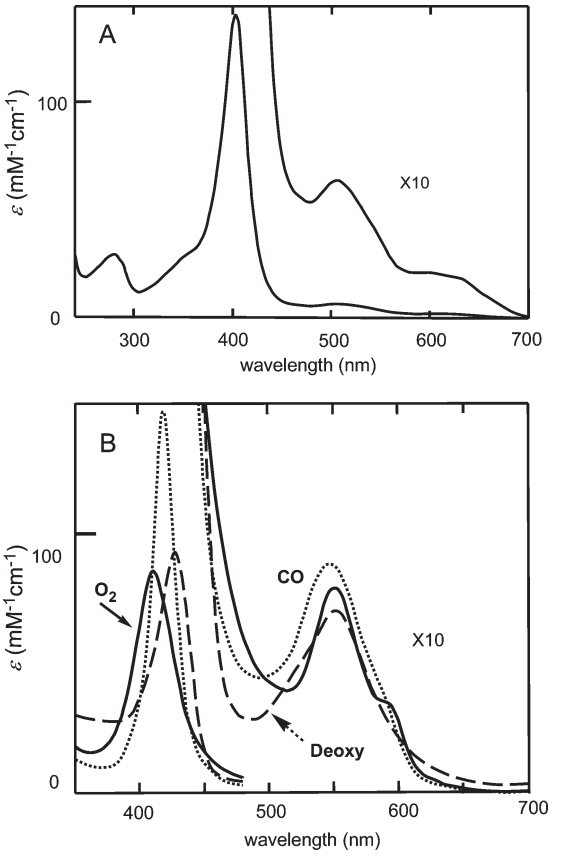

FIGURE 3: Electronic absorption spectra. (A) Ferric aquomet Mb**1** in 0.1 M Tris at pH 7.0 and 20 °C. (B) Ferrous deoxy (– – –), O_2 (—), and CO (· · ·) derivatives of Mb**1** in 0.1 M Tris at pH 7.0 and 20 °C.

As shown in Figure 2, the atom displacement from planarity of heme **1** was ~3-fold larger in magnitude compared to that of heme **2**.

Reconstituted Mbs. Hemes **1** and **2** were normally coupled with apoMb to afford the reconstituted Mb. The electronic absorption spectra of Mb**2** have been partly characterized by Chang and co-workers (*23*). Figure 3 shows the absorption spectrum of ferric Mb**1** with a Soret peak at 403 nm and visible absorption bands at 506, 600, and 630 nm. The magnitude of the Soret peak is 4.9-fold higher than that of the 280 nm globin band to indicate a high purity of the reconstituted protein. The magnitude of the Soret band was clearly decreased at 403 nm and increased at 423 nm with the isosbestic points at 355 and 413 nm with the increase in pH from 7 to 10. We estimated the midpoint of the transition to be a pK of 9.0 ± 0.1 for Mb**1** in 10 mM Tris at 20 °C. We also observed the large spectral changes with pH for ferric Mb**2** and obtained a a pK of 9.1 ± 0.1 under the same condition (results not shown).

Several small ligands such as CN^-, N_3^-, F^-, and imidazole are routinely used to asses the properties of hemoproteins. The visible absorption spectra and the ligand affinities are summarized in Tables S1 and S2 of the Supporting Information. These tables indicate that the Mb**1** derivatives, as compared with the Mb**2** complexes, uniformly exhibit a bathochromic shift of ~10 nm. The tables further show that the ligand affinities of the ferric Mbs are larger in Mb**1** than in Mb**2**. For instance, the affinities of F^- and imidazole in Mb**1** are enhanced by 15- and 30-fold, respectively.

The ferrous deoxy complexes of Mb**1** and Mb**2** were functionally active in binding O_2 and CO. Figure 3 shows the absorption spectra of ferrous Mb**1** derivatives, and the spectral results are compiled in the same tables. Ferrous Mb**1** exhibited absorption bands shifted to the red by ~10 nm relative to those in Mb**2**, in agreement with the results for the ferric derivatives.

Paramagnetic NMR. We examined the proton NMR spectra to elucidate further the coordination environment of Mb**1** and Mb**2**. The spectra of the aquomet derivatives are illustrated in panels A and B of Figure 4. As expected from the heme structures, the six heme-methyl signals appeared at 80.3, 77.5, 74.6, 66.5, 60.0, and 51.8 ppm in Mb**1** and at 87.6, 82.3, 78.2, 68.1, 62.1, and 60.1 ppm in Mb**2**. The large heme-methyl shifts indicate the ferric high-spin ($S = {}^5/_2$) state of the heme iron (*26*). The spread of the methyl peaks, 28.5 ppm in Mb**1** and 27.5 ppm in Mb**2**, is almost identical in both proteins, suggesting the similarity of iron electronic states (*27*). In the upfield region, the −4.9 and −6.1 ppm signals, assigned to the two methyls from the Val11 group (*28*), were observed in both Mbs. There was no signal above −20 ppm. When the aquomet Mbs were analyzed in the H_2O solvent, exchangeable signals appeared at 105.2 ppm for Mb**1** and 102.1 ppm for Mb**2** (Figure 4C). In the NMR spectrum for native Mb (*29*), these exchangeable peaks were assigned to the NH signals of the proximal histidine. The heme methyl shifts were markedly pH-dependent (Figure 4D). The spectra at alkaline pD show that the methyl signal moved upfield with line broadening to 77.9, 75.2, 72.4, 64.6, 58.5, and 50.5 ppm in Mb**1** and 80.0, 75.7, 72.3, 64.4, 57.6, and 57.6 ppm in Mb**2**. In Figure 4E, the NMR signals of the ferrous deoxy complexes are presented. The exchangeable signals, assigned to the proximal

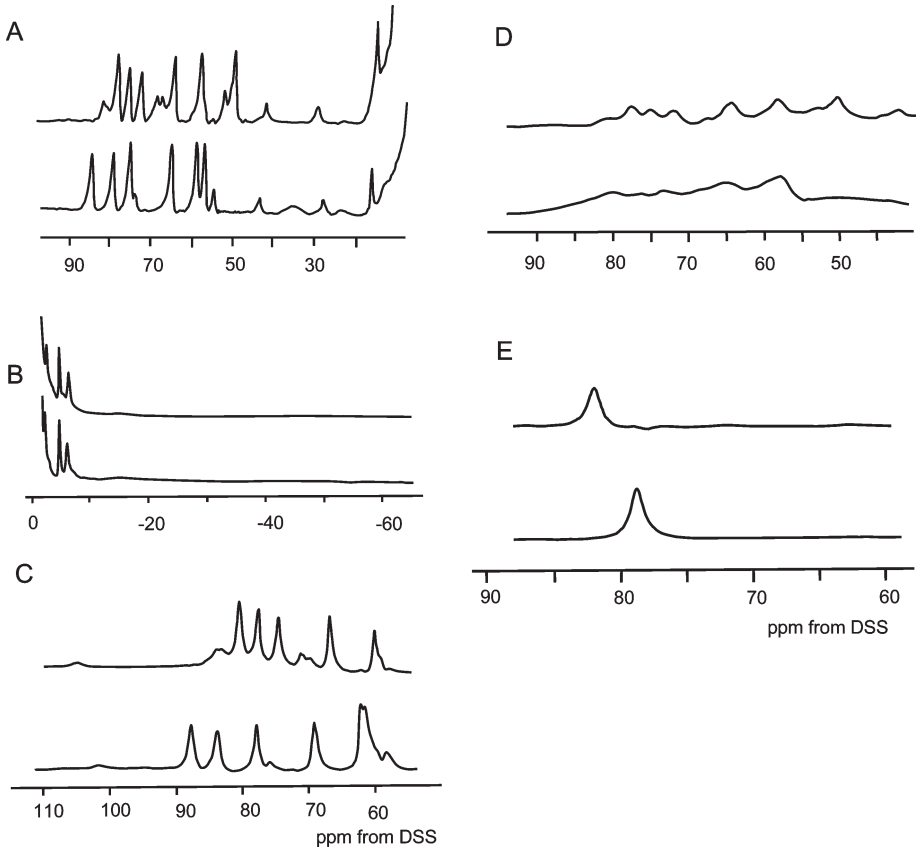

FIGURE 4: Proton NMR spectra. (A) Ferric aquomet Mb**1** and Mb**2** in 0.1 M Tris in D_2O at 20 °C and pD 7.0. (B) Upfiled region of the aquomet Mb spectrum. (C) Ferric aquomet Mb**1** and Mb**2** in 0.1 M Tris at pH 7.0 and 20 °C in a 1:10 (v/v) D_2O/H_2O mixture. Peaks at 105.2 and 102.1 ppm are exchangeable signals. (D) Mb**1** at pD 8.2 and Mb**2** at pD 8.5 in 0.1 M Tris and D_2O at 20 °C. (E) Exchangeable NH signal of the proximal histidine in ferrous deoxy Mb**1** and Mb**2** in 0.1 M Tris at 20 °C and pH 7.0 in a 1:10 (v/v) D_2O/H_2O mixture. The top and bottom traces show data for Mb**1** and Mb**2**, respectively, in panels A−D.

histidine (*30*), appeared at 82.0 ppm for Mb**1** and 78.8 ppm for Mb**2**.

EPR Spectra. Figure 5 shows the EPR spectra of the aquomet derivatives of Mb**1** and Mb**2**. The spectrum found in Mb**2** with $g = 6.0$ and 2.0 signals was of axial type and almost identical with that of native Mb (*31*). The spectrum of Mb**1**, also characteristic of ferric high-spin heme, showed slightly split $g = 5.94$ and 5.76 signals reflecting a decreased level of symmetry of the iron center. In the ferrous NO complexes, a striking difference was noted. Mb**1** showed the three-line signal with a hyperfine coupling constant (^{NO}A) of 1.6 mT in addition to the six-coordinate NO heme signal. The three-line pattern is peculiar to five-coordinate NO heme (*32*) and suggests a cleavage of the iron−histidine bond. The ratio of the five- and six-coordinate species in Mb**1** was estimated to be approximately 50:50. On the other hand, Mb**2** exhibited the EPR spectrum of typical six-coordinate NO heme (*32*).

Ferric Azide Mb. The iron-bound azide in ferric hemoprotein is a useful IR probe because it monitors the iron spin-state equilibrium between the high-spin ($S = {}^5/_2$) and low-spin ($S = {}^1/_2$) states (*33*, *34*), and because the equilibrium reflects the displacement of iron from heme plane. The IR spectra of the azide ions in Mb**1** and Mb**2** are provided in Figure 6A. They exhibited split IR bands, in agreement with the presence of two spin states. The peaks at 2047 (2046) and 2025 (2024) cm^{-1} in Mb**1** (Mb**2**) have been assigned to the high- and low-spin complexes, respectively (*33*, *34*). Consistent with the assignment, the low-spin IR peaks for the low-spin species were intensified at lower temperatures (results not shown). Since the two bands have almost identical extinction coefficients (*33*), the integrated peak intensities are directly correlated to the spin isomer populations. We calculated, from the peak intensities of the IR spectra, the population of the high-spin species to be 9% for Mb**1** and 47% for Mb**2**.

The ^1H NMR spectra of azidomet Mb**1** and Mb**2** are compared in Figure 6B. The heme methyl signals were located at 27.1, 23.2, 17.1, 15.8, 10.0, and 7.3 ppm in Mb**1** and 33.5, 33.2, 26.9, 22.8, 21.8, and 16.3 ppm in Mb**2**. On the basis of the established NMR diagnostic that low-spin heme exhibits smaller methyl shifts than the high-spin heme (*26*), the upfield bias of the methyl signals in Mb**1** shows a larger low-spin population in Mb**1**. The larger low-spin population in Mb**1** relative to Mb**2** inferred from the IR and NMR data is also consistent with the lower visible absorption band at 620 nm in Mb**1** (Tables S1 and S2 of the Supporting Information) since the visible band has been empirically employed as a high-spin marker of ferric heme iron (*35*).

O_2 Binding. We analyzed the oxygen binding in Mb**1** and Mb**2** to examine the functional consequence of the heme deformation. The oxygen affinity of Mb**2** has been reported to be $8.1 \times 10^6\ M^{-1}$ (K) or 0.07 mmHg (P_{50}) (*23*).[2] The P_{50} of Mb**2**,

[2]The oxygen affinity of Mb**2** (P_{50}) has been erroneously estimated to be 0.40 mmHg in ref *25*. The P_{50} value in Table 1 of ref *25* is identical with that of native Mb. From the reported k_{on} and k_{off} constants of oxygen binding (*25*), we obtained a P_{50} of 0.07 mmHg for Mb**2**. The recalculated P_{50} suggests that Mb**2** has a higher oxygen affinity than native Mb. This is in agreement with the result that the hemoglobin containing heme **2** exhibits a higher oxygen affinity than native hemoglobin (*19*).

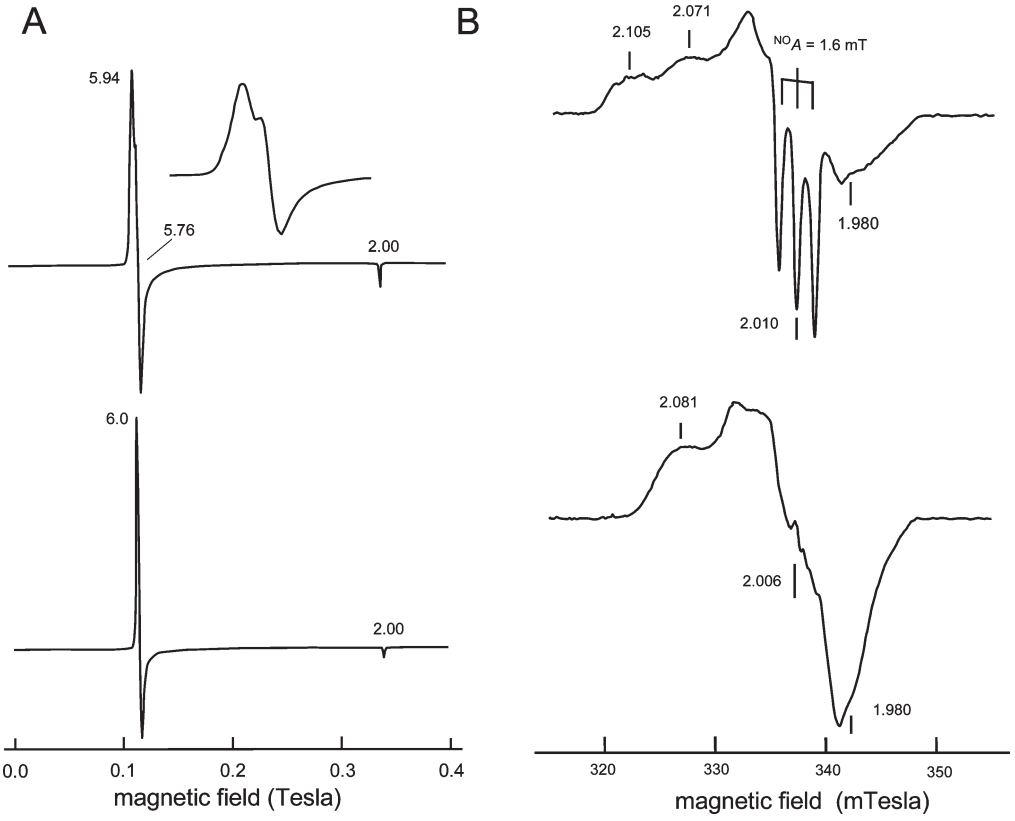

FIGURE 5: EPR spectra. (A) Ferric aquomet Mb**1** and Mb**2** in 0.1 M Tris at pH 7.0 and 5 K. The inset in the top trace denotes the expanded $g = 6$ region. (B) Ferrous NO Mb**1** and Mb**2** in 0.1 M Tris at pH 7.0 and 35 K. The top and bottom traces show data for Mb**1** and Mb**2**, respectively, in panels A and B.

smaller than the P_{50} value of 0.73 mmHg of native Mb (*36*), indicates the increase in the oxygen affinity after replacement of the electron-withdrawing vinyl substituents with the electron-donating methyl groups (*19*, *23*, *36*). The Hill plots of the oxygen equilibrium for Mb**1** with a P_{50} of 1.79 ± 0.01 mmHg are illustrated in Figure S1 of the Supporting Information. Comparison of the oxygen affinities in Tables S1 and S2 indicates that Mb**1** exhibits an affinity as much as 25-fold lower than that of Mb**2**.

CO Binding. To elucidate further the functional outcome of the heme distortion, CO binding was examined. The optical CO titration to deoxy Mb**1** is illustrated in Figure 7, where the CO affinity [$K = (5.90 \pm 0.07) \times 10^4$ M^{-1}, or $P_{50} = 12.4 \pm 0.2$ mmHg] was obtained. The absorption increase of CO Mb**1** after flash photolysis was clearly monophasic at 418 nm, and the curve of CO recombination was characterized with a value of 2.50×10^3 s^{-1}. From the equilibrium and kinetic experiments and the CO concentration of 1.0 mM in water at 20 °C, we obtained the following rate constants for Mb**1**: $k_{on} = 2.40 \times 10^6$ M^{-1} s^{-1}, and $k_{off} = 40.0$ s^{-1}. Chang and co-workers have reported the CO binding to Mb**2** under similar conditions (*23*). According to their results, the CO binding to Mb**2** is accompanied by the following values: $k_{on} = 6.7 \times 10^5$ M^{-1} s^{-1}, $k_{off} = 0.022$ s^{-1}, $K = 3.1 \times 10^7$ M^{-1} or $P_{50} = 0.026$ mmHg. It is to be noted that the CO affinity of Mb**1** is 480-fold smaller than that of Mb**2**, and that the markedly diminished CO affinity comes entirely from the increase in the k_{off} rate.

DISCUSSION

Influence of the meso-Ethyl Substituent. Bulky *meso*-substituents on the porphyrin ring deform the planar porphyrin (*1*, *3*, *4*). The deformed porphyrin and metalloporpohyrin decrease the energy gap between the highest-occupied and lowest-unoccupied molecular orbitals to induce the bathochromic shift of the visible absorption bands. The proof for the relationship between nonplanarity and absorption band shifts has been provided by molecular orbital calculations (*2*).

The ferric chloride derivatives of hemes **1** and **2** exhibited Soret maxima at 380 and 383 nm, respectively. The difference in the Soret peaks positions of the hemes in the heme pocket is ~10 nm (Tables S1 and S2 of the Supporting Information). These difference are small but significant. The red-shifted Soret maximum of ferric heme **1** suggests a heme distortion. The ethyl side chain in heme **1**, despite the small bulk, is capable of deforming the heme plane through a steric repulsion with the adjacent heme methyls. When we placed an ethyl group on α *meso*-carbon of heme **1** in a planar conformation, the CH_2 (*meso*-ethyl)-CH_3 (heme methyl) separation is only 2.70 Å. Since the van der Waals radius of methylene and methyl groups is 2.0 Å (*37*), there is significant van der Waals strain between the CH_2 (*meso*-ethyl) and CH_3 (heme methyl) groups. In the energy-minimized deformed structure of heme **1**, the CH_2 (*meso*-ethyl)−CH_3 (heme methyl) separation is increased to 3.18 Å to relieve the strain. It could be argued, however, that that heme distortion may arise from the altered heme−protein contacts by the ethyl substituent, rather than the van der Waals strain between the CH_2 (*meso*-ethyl) and CH_3 (heme methyl) groups in heme. This possibility is excluded by the observation for the Mb reconstituted with octaethylheme (*38*). The Mb exhibits visible absorption maxima that are almost identical with those of Mb**2** containing a nondistorted heme, suggesting that the octaethylheme bearing bulky ethyl groups is not distorted in protein.

It has been reported for core contracted ferric hemes that the mixing of the intermediate-spin state ($S = {}^3/_2$) with the high-spin state ($S = {}^5/_2$) is frequently observed (*4*−*7*). The $g = 6$ EPR

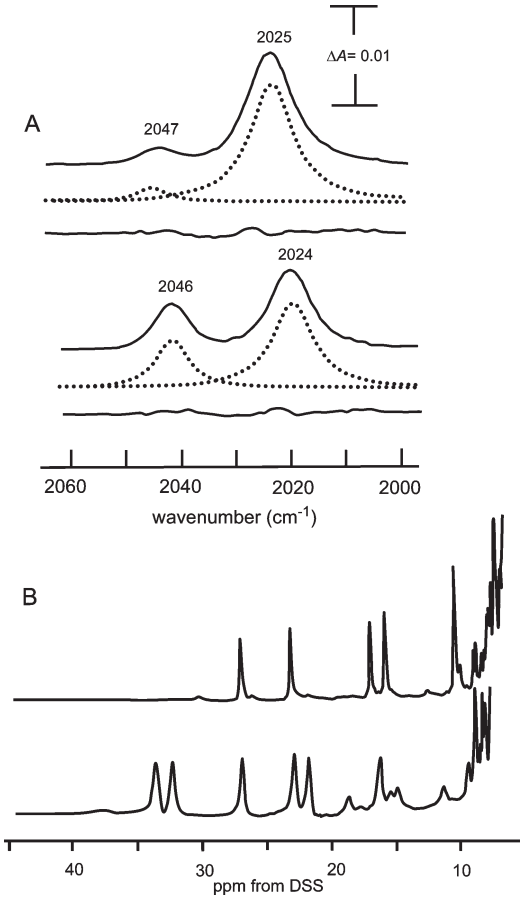

FIGURE 6: Ferric azidomet Mbs. (A) IR spectra of Mb**1** and Mb**2** in 0.1 M Tris at pH 7.0 and 20 °C. The dotted curves are calculated fittings, and the residues are also given. (B) Proton NMR spectra of Mb**1** and Mb**2** in 0.1 M Tris at pD 7.0 and 20 °C. The top and bottom traces show data for Mb**1** and Mb**2**, respectively, in panels A and B.

signal, characteristic of the pure high-spin state, gradually shifts toward a $g = 4$ signal with an increasing population of the intermediate-spin state. The possibility of mixing of the $S = {}^3/_2$ state in aquomet Mb**1** appears to be negligibly small because a shift of the $g = 6$ signal to the higher magnetic field is not evident in the EPR spectrum in Figure 5. The slightly split $g = 6$ band may be correlated with the rhombic symmetry-breaking perturbation, rather than the mixing of the $S = {}^3/_2$ state. The EPR result in Figure 5 indicates the pure high-spin state for aquomet Mb**1**, and the negligible core contraction.

Iron Displacement in Deformed Heme. Another notable result in Tables S1 and S2 of the Supporting Information is the fact that the ligand affinities of metMb**1** are uniformly larger than those of metMb**2**. The observation suggests weaker water coordination in metMb**1** than in metMb**2**. However, it may be argued that the higher ligand affinities in Mb**1** reflect the absence of the coordinating water molecule. The presence of the iron-bound water in metMb**1** is supported by the proton NMR spectrum. The spectrum of metMb**1** (Figure 4B) exhibits no NMR signal in the −20 to −60 ppm region. If metMb**1** were five-coordinate, a broad *meso*-proton signal should be observed there. The absence of the *meso*-proton signal in metMb**1** suggests the six-coordinate structure with an iron-bound water molecule. The six-coordinate aquomet structure for metMb**1** is further supported by the NMR spectrum at alkaline pD (Figure 4D). The heme methyl shift of alkaline metMb**1** can be attributed to the rapid proton dissociation of the heme-linked distal histidine, rather than the slow ligand exchange of the sixth ligand on the heme iron, and hence is assigned to the proton dissociation of coordinating water from hydroxide (*39*). Thus, the NMR results in panels B and D of Figure 4 confirm the presence of iron-bound water in metMb**1** at neutrality.

The weaker water binding in metMb**1** could reflect a stronger iron−proximal histidine bond. The rationale for this interpretation comes from the general theory of the donor−acceptor interactions (*40*). According to the theory, the stronger iron−histidine bond weakens the iron−water bond at the *trans* axial site, and higher ligand affinity of aquomet Mb**1** as Tables S1 and S2 indicate. The stronger iron−histidine interaction is supported by NMR. Figure 4A shows that the average paramagnetic shift of the heme-methyl signals is smaller by 5 ppm in metMb**1** than in metMb**2**. Since the shift of the ferric high-spin hemoprotein is predominantly contributed by the iron spin transfer through the Fe−N(pyrrole) bonds (*26*), the smaller heme-methyl shift of metMb**1** comes from decreased spin density on the methyl groups. The decreased rate of spin transfer reflects the longer Fe−N(pyrrole) bond, consistent with the larger iron displacement caused by the stronger iron−histidine interaction in metMb**1**. The exchangeable NH signals of the proximal histidine appeared at 105.2 ppm in metMb**1** and at 102.1 ppm in metMb**2** (Figure 4C). The larger chemical shift of the proximal histidine signal suggests the enhanced iron−histidine interactions. The stronger axial interaction in Mb**1** is further supported by the proton NMR in the ferrous state. Figure 4E shows that deoxy Mb**1** (82.0 ppm) exhibits the exchangeable NH signal of the proximal histidine at a lower field than Mb**2** (78.8 ppm). The NH shift of Mb**2** is almost identical with 77.8 ppm in native Mb (*30*). Since the NH shift arises from iron-spin transfer to the proximal imidazole through the iron−histidine bond (*30*), the larger NH shift in Mb**1** indicates the stronger iron−histidine bond in Mb**1**. It could be suggested, however, that the larger NH shift of Mb**1** is caused by a conformational change of the proximal imidazole due to altered heme peripheral contacts by the *meso*-ethyl group. This possibility is less likely because the proton NMR of ferrous deoxy Mb bearing octaethylheme exhibits the NH signal at 78.5 ppm (*38*), close to 77.8 ppm in native Mb (*30*), despite the intensively modified heme−globin contacts. It is thus likely that the larger NH shift in Mb**1** reflects stronger iron−histidine bonds caused by the heme deformation.

Azide Complex. As the NMR in Figure 4 implies, the iron atom in aquomet Mb**1** is more displaced toward the proximal histidine. Upon coordination of azide, the iron shifts toward the azide (*41*). The larger iron displacement in aquomet Mb**1** toward the proximal site could make the iron movement on azide binding less favorable. Thus, the iron atom falls into the heme plane in Mb**1**, while the iron in Mb**2** is displaced toward azide. This results in shorter iron−N(pyrrole) bonds, the stronger equatorial ligand field of heme iron, and the bias of spin equilibrium to the low-spin form in azidomet Mb**1**. The IR and NMR results for Mb**1** in Figure 6 support the stronger equatorial ligand field and larger low-spin population. From the analysis for mutant Mbs, the heme distal side effect is suggested to be another determinant of the iron spin equilibrium of azidomet Mb (*42*). However, the situation cannot be applied to our case because the globin is native in both Mb**1** and Mb**2**.

CO and NO Derivatives. It has been proposed that only marginal distortion is produced by a small *meso*-substituent in a nona-substituted porphyrin plane (*4*). However, this is not always true for the heme placed in a protein matrix. Heme **1** with

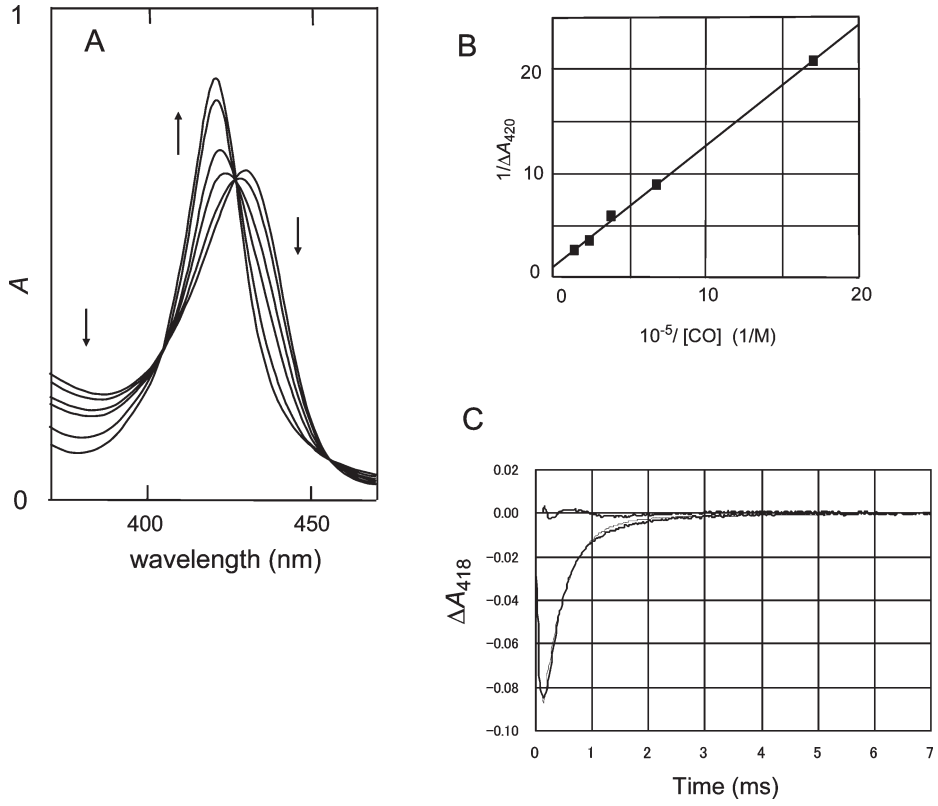

FIGURE 7: CO binding to ferrous Mb**1**. (A) Soret absorption changes. [CO] = 0−0.59, 1.5, 2.6, 4.1, and 7.1 μM as indicated by the arrows in 0.1 M Tris at pH 7.0 and 20 °C. (B) Analysis of the Soret absorption changes. (C) Kinetic trace after flash photolysis in 0.1 M Tris at pH 7.0 and 20 °C.

a *meso*-ethyl substituent obviously influences the Mb function, and the O_2 and CO affinities are significantly decreased when compared with those of heme **2** without an ethyl group. The proton MNR spectrum in Figure 4 shows that the proximal histidine pulls more of the iron to cause a stronger iron−histidine bond in Mb**1**. The stronger iron−histidine interaction is associated with a greater iron displacement from the plane of heme **1**. The situation explains the anomaly in CO binding. The CO affinity of Mb**1** is extremely low, and the decreased CO affinity solely came from the increase in the k_{off} rate (Figure 7). Since the CO is a π-acceptor, the enhanced iron displacement toward the proximal histidine causes less overlap of the iron d_π orbitals with CO π orbitals to weaken the iron−CO bond. It is worth pointing out that the iron−histidine bond is broken in some fraction of NO Mb**1** (Figure 4). This may arise from synergetic effects of the labile iron position in heme **1** and the excellent π-accepting ability of NO.

Unique Profile of Inherently Deformed Heme. The displacement of iron from the heme plane toward the proximal histidine reduces the ligand affinity of ferrous heme. This is the view established for ordinary undistorted heme. This work demonstrates that the iron displacement is enhanced on heme deformation. The direct comparison of Mb**1** with Mb**2** reveals the characteristic behavior of the iron in distorted heme **1**. When compared with Mb**2**, Mb**1** has the higher and lower ligand affinities in the ferric and ferrous states, respectively. The apparently opposed results between the ferric and ferrous states are consistently explained in terms of the enhanced iron displacement from the plane of heme **1**. In NO Mb**1**, the displaced iron tends to be pulled by NO, a very strong π-accepting ligand, to cleave the iron−histidine bond.

We have previously reported that the O_2 and CO affinities of the Mb reconstituted with iron corrphycene (*43*, *44*) or oxypyriporphyrin (*45*) are notably low. The molecular shapes of these macrocycles are trapezoidal and rhomboid, respectively. We note that the functional outcomes of heme **1** are closely similar to iron corrphycene and iron oxypyriporphyrin despite the dissimilar molecular structures. A common denominator that regulates the iron reactivity must be present. In deformed heme **1**, the four pyrrole planes are twisted away from the heme mean plane (Figure 2). In this situation, the overlap between the σ-lobes on four pyrrole nitrogens and the iron $d_{x^2-y^2}$ orbital with orthogonal lobes becomes less favorable, and the iron−N(pyrrole) bonds are weakened. The same may be also true for the iron complexes of corrphycene (*44*) and oxypyriporphyrin (*45*) with non-square cyclic pyrroles. The destabilized equatorial iron−N(pyrrole) bonds thus make the iron atom more susceptible to the axial pull effect by the proximal histidine or by NO. Thus, the decreased O_2 and CO affinities and the iron−imidazole cleaved bond by NO in protein-bearing deformed hemes are explained.

Relevance for Different Hemoproteins. We note that Mb**1** is quite similar with guanylate cyclase, an NO-responsive signaling hemoprotein (*46*, *47*). The enzyme has a highly deformed protoheme, and the proximal histidine coordinates to the heme iron (*10*). Curiously, the protoheme has no measurable affinity for oxygen, and the CO affinity is extremely low (*9*) despite the vacant sixth coordination site. The iron−histidine bond in guanylate cyclase is broken upon NO binding (*48*, *49*). The decreased CO affinity of guanylate cyclase is characterized with an unusually fast k_{off} rate (*50*). These behaviors in the heme enzyme are mimicked by Mb**1** contaning the distorted heme. The results of Mb**1** may indicate that the anomalies of the protoheme in guanylate cyclase reflect the heme distortion (*10*, *50*). Although Mb and guanylate cyclase perform different functions, the consequences by heme distortion appear to be related to each other. The similarity could suggest the utility of the results obtained for

Mb**1** to the functional analysis of hemoproteins containing deformed heme structures. Hemoglobin has more distorted hemes than Mb (*1*). In view of the results for Mb**1** described above, it may be attractive to speculate that the increased heme distortion partly plays a role in the lower affinity for O_2 and CO in hemoglobin.

ACKNOWLEDGMENT

We thank the Institute for Molecular Science, Okazaki, Japan, for supporting the EPR measurements.

SUPPORTING INFORMATION AVAILABLE

Hill plots of O_2 binding to Mb**1**, visible absorption spectral data, and ligand affinities for Mb**1** and Mb**2**. This material is available free of charge via the Internet at http://pubs.acs.org.

REFERENCES

1. Shelnutt, J. A., Song, X.-Z., Ma, J.-G., Jia, S.-L., Jentzen, W., and Medforth, C. J. (1998) Nonplanar porphyrins and their significance in proteins. *Chem. Soc. Rev. 27*, 31–41.
2. Haddad, R. E., Gazeau, S., Pecaut, J., Marchon, J.-C., Medforth, C. J., and Shelnutt, J. A. (2003) Origin of the red shifts in the optical absorption bands of nonplanar tetraalkylporphyrins. *J. Am. Chem. Soc. 125*, 1253–1263.
3. Senge, M. O. (2000) Highly substituted porphyrins. In The Porphyrin Handbook (Kadish, K. M., Smith, K. M., and Guilard, R., Eds.) Vol. *1*, pp 239−347, Academic Press, New York.
4. Nakamura, M. (2006) Electronic stuructures of highly deformed iron(III) porphyrin complexes. *Coord. Chem. Rev. 250*, 2271–2294.
5. Schünemann, V., Gerdan, M., Trautwein, A. X., Haoudi, N., Mandon, D., Fischer, J., Weiss, R., Tabarde, A., and Guilard, R. (1999) The 5/2,3/2 spin admixture in the chloroiron(III) derivative of the sterically crowded 2,3,7,8,12,13,17,18-octaethyl-5,10,15,20-tetraphenylporphyrin. *Angew. Chem., Int. Ed. 38*, 3181–3183.
6. Weiss, R., Gold, A., and Terner, J. (2006) Cytochrome *c′*. *Chem. Rev. 106*, 2550–2579.
7. Maltempo, M., and Moss, T. H. (1976) The spin 3/2 state and quantum spin mixtures in haem proteins. *Q. Rev. Biophys. 9*, 181–215.
8. Neya, S., Takahashi, A., Ode, H., Hoshino, T., Hata, M., Ikezaki, A., Ohgo, Y., Takahashi, M., Hiramatsu, H., Kitagawa, T., Furutani, Y., Kandori, H., Funasaki, N., and Nakamura, M. (2007) Magnetic and infrared properties of the azide complex of (2,7,12,17-tetrapropylporphycenato)iron(III). *Eur. J. Inorg. Chem.,* 3188–3194.
9. Neya, S., Takahashi, A., Ode, H., Hoshino, T., Ikezaki, A., Ohgo, Y., Takahashi, M., Furutani, Y., Lórenz-Fonfría, V. A., Kandori, H., Funasaki, N., Nakamura, M., Hiramatsu, H., Kitagawa, T., Teraoka, J., Funasaki, N., and Nakamura, M. (2008) Electronic properties of five-coordinate of azide complex of non-planar iron(III) porphyrin. *Bull. Chem. Soc. Jpn. 81*, 136–141.
10. Pellicena, P., Karow, D. S., Boon, E. M., Marletta, M. A., and Kuriyan, J. (2004) Crystal structure of an oxygen-binding heme domain related to soluble guanylate cyclases. *Proc. Natl. Acad. Sci. U.S.A. 101*, 12854–12859.
11. La Mar, G. N., de Ropp, J. S., Smith, K. M., and Langry, K. C. (1983) Determination by ^{1}H NMR of the orientation of modified hemes incorporated into horseradish peroxidase. *J. Am. Chem. Soc. 105*, 4576–4580.
12. Smith, K. M., and Minnetian, O. M. (1986) Cyclizations of 1′,8′-dimethyl-*a,c*-biladine salts to give porphyrins: A study with various oxidizing agents. *J. Chem. Soc., Perkin Trans. 1,* 277–280.
13. Maruyama, K., Nagata, T., and Osuka, A. (1988) Study on 5,15-dialkylporphyrins interconversion between two conformers in solution. *J. Phys. Org. Chem. 1*, 63–73.
14. Robinson, J. A., McDonald, E., and Battersby, A. B. (1985) Biosynthesis of porphyrins and related macrocycles. *J. Chem. Soc., Perkin Trans. 1,* 1699–1709.
15. Hambright, P. (1975) Dynamic coordination chemistry of metalloporphyrins. In Porphyrins and Metalloporphyrins (Smith, K. M., Ed.) pp 233−278, Elsevier, Amsterdam.
16. Adler, D., Longo, F., Kampas, F., and Kim, J. (1979) On the preparation of metalloporphyrins. *J. Inorg. Nucl. Chem. 32*, 2443–2445.
17. Fuhrhop, J.-H., and Smith, K. M. (1975) Laboratory methods. In Porphyrins and Metalloporphyrins (Smith, K. M., Ed.) pp 757−869, Elsevier, Amsterdam.
18. Asakura, T. (1978) Hemoglobin porphyrin modification. *Methods Enzymol. 52*, 447–455.
19. Seybert, D. W., Moffat, K., Gibson, Q. H., and Chang, C. K. (1977) Electronic and steric factors affecting ligand binding. *J. Biol. Chem. 252*, 4225–4231.
20. Frisch, M. J., Trucks, G. W., Schlegel, H. B., Scuseria, G. E., Robb, M. A., Cheeseman, J. R., Montgomery, J. A., Jr., Vreven, T., Kudin, K. N., Burant, J. C., Millam, J. M., Iyengar, S. S., Tomasi, J., Barone, V., Mennucci, B., Cossi, M., Scalmani, G., Rega, N., Petersson, G. A., Nakatsuji, H., Hada, M., Ehara, M., Toyota, K., Fukuda, R., Hasegawa, J., Ishida, M., Nakajima, T., Honda, Y., Kitao, O., Nakai, H., Klene, M., Li, X., Knox, J. E., Hratchian, H. P., Cross, J. B., Bakken, V., Adamo, C., Jaramillo, J., Gomperts, R., Stratmann, R. E., Yazyev, O., Austin, A. J., Cammi, R., Pomelli, C., Ochterski, J. W., Ayala, P. Y., Morokuma, K., Voth, G. A., Salvador, P., Dannenberg, J. J., Zakrzewski, V. G., Dapprich, S., Daniels, A. D., Strain, M. C., Farkas, O., Malick, D. K., Rabuck, A. D., Raghavachari, K., Foresman, J. B., Ortiz, J. V., Cui, Q., Baboul, A. G., Clifford, S., Cioslowski, J., Stefanov, B. B., Liu, G., Liashenko, A., Piskorz, P., Komaromi, I., Martin, R. L., Fox, D. J., Keith, T., Al-Laham, M. A., Peng, C. Y., Nanayakkara, A., Challacombe, M., Gill, P. M. W., Johnson, B., Chen, W., Wong, M. W., Gonzalez, C., and Pople, J. A. (2004) Gaussian 03, Gaussian, Inc., Wallingford, CT.
21. Imai, K. (1981) Measurement of accurate oxygen equilibrium curves by an automatic oxygenation apparatus. *Methods Enzymol. 76*, 438–449.
22. Hayashi, A., Suzuki, T., and Shin, M. (1973) Enzymic reduction system for metmyoglobin and methemoglobin, and its application to functional studies of oxygen carriers. *Biochim. Biophys. Acta 310*, 309–316.
23. Chang, C. K., Ward, B., and Ebina, S. (1984) Kinetic study of CO and O_2 binding to horse heart myoglobin reconstituted with synthetic hemes lacking methyl and vinyl side chains. *Arch. Biochem. Biophys. 231*, 366–371.
24. König, D. F. (1965) The structure of α-chlorohemin. *Acta Crystallogr. 18*, 663–673.
25. Scheidt, W. R., and Reed, C. (1981) Spin state/stereochemical relationship in iron porphyrins. *Chem. Rev. 81*, 543–555.
26. La Mar, G. N., and Walker, F. A. (1979) Nuclear magnetic resonance of paramagnetic metalloporphyrins. In The Porphyrins (Dolphin, D., Ed.) Vol. *4*, pp 61−157, Academic Press, London.
27. Budd, D. L., La Mar, G. N., Langry, K. C., Smith, K. M., and Nayyir-Mazhir, R. (1979) ^{1}H NMR study of high-spin ferric natural porphyrin derivatives as models of methemoproteins. *J. Am. Chem. Soc. 101*, 6091–6096.
28. La Mar, G. N., Budd, D. L., Smith, K. M., and Langry, K. C. (1980) Nuclear magnetic resonance of high-spin ferric hemoproteins. *J. Am. Chem. Soc. 102*, 1822–1827.
29. La Mar, G. N., and de Ropp, J. S. (1979) Assignment of exchangeable proximal histidine resonance in high-spin ferric hemoproteins. *Biochem. Biophys. Res. Commun. 90*, 36–41.
30. La Mar, G. N., Budd, D. L., and Goff, H. (1977) Assignment of proximal histidine proton NMR peaks in myoglobin and hemoglobin. *Biochem. Biophys. Res. Commun. 77*, 104–110.
31. Palmer, G. (1979) Electron paramagnetic resonance of hemoproteins. In The Porphyrins (Dolphin, D., Ed.) Vol. *4*, pp 313−353, Academic Press, New York.
32. Maxwell, J. C., and Caughey, W. S. (1976) An infrared study of NO bonding to heme B and hemoglobin A. *Biochemistry 15*, 388–396.
33. Alben, J. O., and Fajer, L. Y. (1972) Infrared studies of azide bound to myoglobin and hemoglobin. *Biochemistry 11*, 842–847.
34. Neya, S., Chang, C. K., Okuno, D., Hoshino, T., Hata, M., and Funasaki, N. (2005) Control of iron(III) spin-state in the model complexes of azide hemoprotein by porphycene, corrphycene, and hemiporphycene macrocycles. *Inorg. Chem. 44*, 1193–1195.
35. Brill, A. S., and Williams, R. J. P. (1961) The absorption spectra, magnetic moments and the binding of iron in some hemoproteins. *Biochem. J. 78*, 246–253.
36. Sono, M., Smith, P. D., McCray, J. A., and Asakura, T. (1976) Kinetic and equilibrium studies on the reactions of heme-substituted horse heart myoglobins with oxygen and carbon monoxide. *J. Biol. Chem. 251*, 1418–1426.
37. Gordon, A. J., and Ford, R. A., Eds. (1972) The Chemist's Companion, p 109, John Wiley & Sons, New York.
38. Neya, S., Funasaki, N., and Imai, K. (1988) Structure and function of the myoglobin containing octaethylhemin as a prosthetic group. *J. Biol. Chem. 263*, 8810–8815.

39. Iizuka, T., Ogawa, S., Inubushi, T., Yonezawa, T., and Morishima, I. (1974) NMR studies of hemoproteins: pH dependence of ferric horseradish peroxidase and horse heart myoglobin. *FEBS Lett. 64*, 156–158.
40. Gutmann, V. (1975) Empirical approach to molecular interactions. *Coord. Chem. Rev. 15*, 203–237.
41. Zhang, Y., Hallows, W. A., Ryan, W. J., Jones, J. G., Carpenter, G. B., and Sweigart, D. A. (1994) Models for steric interactions in heme proteins. *Inorg. Chem. 33*, 3306–3312.
42. Bogmil, R., Hunter, C. L., Maurus, R., Tang, H.-L., Lee, H., Lloyd, E., Brayer, G. D., Smith, M., and Mauk, A. G. (1994) FTIR analysis of the interaction of azide with horse heart myoglobin variants. *Biochemistry 33*, 7600–7608.
43. Neya, S., Funasaki, N., Hori, H., Imai, K., Nagatomo, S., Iwase, T., and Yonetani, T. (1999) Functional regulation of myoglobin by iron corrphycene. *Chem. Lett. 28*, 989–990.
44. Neya, S., Nakamura, M., Imai, K., and Funasaki, N. (2001) Functional analysis the iron(II) corrphycene incorporated into the myoglobin heme pocket. *Chem. Pharm. Bull. 49*, 354–346.
45. Neya, S., Suzuki, M., Ode, H., Hoshino, T., Furutani, Y., Kandori, H., Hori, H., Imai, K., and Komatsu, T. (2008) Functional evaluation of iron oxypyriporphyrin in protein heme pocket. *Inorg. Chem. 47*, 10771–10778.
46. Kasarikov, D. N., Young, P., Uversky, V. N., and Garber, N. C. (2001) Human soluble guanylate cyclase. *Arch. Biochem. Biophys. 388*, 185–195.
47. Stone, J. R., and Marletta, M. A. (1994) Soluble guanylate cyclase from bovine lung. *Biochemistry 33*, 5636–5640.
48. Makino, R., Matsuda, H., Obayashi, E., Shiro, Y., Iizuka, T., and Hori, H. (1999) EPR characterization of axial bond in metal center of native and cobalt-substituted guanylate cyclase. *J. Biol. Chem. 274*, 7714–7723.
49. Stone, J. R., and Marletta, M. A. (1995) The ferrous heme of soluble guanylate cyclase. *Biochemistry 34*, 16397–16403.
50. Olea, C., Jr., Boon, E. M., Pellicena, P., Kuriyan, J., and Marletta, M. A. (2008) Probing the function of heme distortion in the H-NOX family. *ACS Chem. Biol. 3*, 703–710.